Physics Letters B 687 (2010) 26–30

Contents lists available at ScienceDirect

Physics Letters B

www.elsevier.com/locate/physletb

One-neutron knockout from $^{24-28}$Ne isotopes

C. Rodríguez-Tajes [a,*], D. Cortina-Gil [a], H. Álvarez-Pol [a], T. Aumann [b], E. Benjamim [a], J. Benlliure [a], M.J.G. Borge [c], M. Caamaño [a], E. Casarejos [a], A. Chatillon [b], K. Eppinger [d], T. Faestermann [d], M. Gascón [a], H. Geissel [b], R. Gernhäuser [d], B. Jonson [e,g], R. Kanungo [f], R. Krücken [d], T. Kurtukian [a], K. Larsson [e], P. Maierbeck [d], T. Nilsson [e], C. Nociforo [b], C. Pascual-Izarra [c], A. Perea [c], D. Pérez-Loureiro [a], A. Prochazka [b], H. Simon [b], K. Sümmerer [b], O. Tengblad [c], H. Weick [b], M. Winkler [b], M. Zhukov [e]

[a] Departamento de Física de Partículas, Universidade de Santiago de Compostela, 15782 Santiago de Compostela, Spain
[b] GSI Helmholtzzentrum für Schwerionenforschung, 64291 Darmstadt, Germany
[c] Instituto de Estructura de la Materia, CSIC, 28006 Madrid, Spain
[d] Physik Department E12, Technische Universität München, 85748 Garching, Germany
[e] Fundamental Fysik, Chalmers Tekniska Högskola, 412 96 Göteborg, Sweden
[f] Astronomy and Physics Department, Saint Mary's University, Halifax, NS B3H 3C3, Canada
[g] PH Department, CERN, 1211 Geneve 23, Switzerland

ARTICLE INFO

Article history:
Received 22 December 2009
Accepted 1 March 2010
Available online 5 March 2010
Editor: M. Doser

Keywords:
Nuclear structure
Neutron-rich nuclei
One-neutron knockout
^{24}Ne
^{25}Ne
^{26}Ne
^{27}Ne
^{28}Ne

ABSTRACT

One-neutron knockout reactions of $^{24-28}$Ne in a beryllium target have been studied in the Fragment Separator (FRS), at GSI. The results include inclusive one-neutron knockout cross-sections as well as longitudinal-momentum distributions of the knockout fragments. The ground-state structure of the neutron-rich neon isotopes was obtained from an analysis of the measured momentum distributions. The results indicate that the two heaviest isotopes, ^{27}Ne and ^{28}Ne, are dominated by a configuration in which a $s_{1/2}$ neutron is coupled to an excited state of the ^{26}Ne and ^{27}Ne core, respectively.

1. Introduction

In recent years, the $N \sim 20$ neutron-rich region of the nuclear landscape has been in the focus of numerous experimental studies, since indications of new structural phenomena such as the disappearance of the $N = 20$ magicity, observed for sodium and magnesium isotopes [1,2], have been found. Different models have attempted to explain the vanishing of the $N = 20$ shell closure, some of them based on *proton-hole* intruder states that originate what is known as the *island of inversion*. Monte Carlo Shell Model calculations [3,4] allowing the mixing of *sd* and *pf* configurations (SDPF-M) provide a reasonable description of the experimental data and predict a wider island of inversion, with the appearance of ground-state intruder configurations at $N = 18$ and low-energy intruder states up to $N = 17$. The vanishing of magicity at $N = 20$ has also been related to a new shell gap at $N = 16$ that occurs for nuclei far from stability [5]. The exotic doubly magic nucleus ^{24}O is a well-known example, where a recent demonstration of an almost pure $1s_{1/2}$ state [6] and the determination of the resonance energy of the lowest lying state, interpreted as the 2^+ level, beautifully confirm its magicity [7].

The proximity of $^{24-28}$Ne isotopes to the island of inversion justifies the investigation of their structure. Earlier experiments carried out for ^{25,26}Ne are consistent with calculations in the *sd* space (USD) and show no evidence of any anomalous behaviour [8–11]. However, when more neutrons are added, SDPF-M calculations [3] are needed to reproduce the experimental data. This is the case for the $3/2^-$ level of ^{27}Ne at 765 keV [8,9,12] and the first excited state of ^{28}Ne, located at 1293 keV, with $I^\pi = 2^+$ [11,12]. We especially point to the work carried out by Terry et al. [9], where ex-

* Corresponding author. Tel.: +34 981563100 13627; fax: +34 981521091.
E-mail address: carme.rodriguez@usc.es (C. Rodríguez-Tajes).

0370-2693/$ – see front matter
doi:10.1016/j.physletb.2010.03.006

perimental results for ^{26,28}Ne one-neutron knockout are presented, showing the importance of intruder states in the ground-state configuration of ^{28}Ne.

In the work presented here, the ground states of $^{24-28}$Ne were explored by means of one-neutron knockout reactions at relativistic energies. The use of a Be target ensured a negligible contribution from Coulomb dissociation. In the high-energy regime, stripping reactions dominate the process [13] and the measurement of the longitudinal-momentum distribution of the knockout fragments was used to identify the orbital angular momentum of the removed neutron. The one-neutron knockout cross-section was also evaluated in order to obtain additional information.

2. Experiment

The experiment was performed in the Fragment Separator (FRS) [14], at GSI (Darmstadt, Germany) [15]. A fully ionised ^{40}Ar primary beam was accelerated in the SIS heavy ion synchrotron up to 700 MeV/nucleon and directed towards a 4 g/cm^2 Be target located at the entrance of the FRS, where, via fragmentation reactions, a cocktail of exotic neutron-rich projectiles was produced. The mean intensity was around 10^{10} Ar-ions/spill, for spills produced within a 20 s period and a length fluctuating between 4 and 6 s. Fig. 1 shows a schematic view of the detector arrangement in the FRS. The neutron-rich projectiles were separated and identified in the first half of the spectrometer, F0–F2. Then, the one-neutron knockout reaction took place at the intermediate focal plane, F2, in a 1720 mg/cm^2 Be target and the analysis of the knockout fragments was performed in the second part of the FRS, F2–F4. The experimental setup allowed a clean selection of the reaction channel based on the identification of both the projectile and knockout fragment. For that purpose, the charge of the nuclei was measured in ionisation chambers (MUSIC). Since the nuclei were fully ionised, the obtained charge was equal to the atomic number. The mass-to-charge ratio was determined from the magnetic rigidity, $B\rho = \gamma m_0 \beta c/q$, and the velocity of each nucleus, β, in order to complete the identification. The $B\rho$ calculation was based on position measurements at the intermediate and final focal planes (TPC) and the velocity was obtained from the time of flight between scintillators (SCI1–SCI2 and SCI2–SCI3).

3. Physical observables

Two inclusive observables were determined in this experiment: the one-neutron knockout cross-section and the longitudinal-momentum distribution of the $A-1$ fragments.

As illustrated in Fig. 2, the calculation of the cross-section was based on the projectile and fragment identification. Two-dimensional plots, Z *versus* A/Z, were used to select the projectile of interest and the corresponding one-neutron knockout fragment. In order to properly evaluate the number of one-neutron knockout events, two corrections were applied to the experimental data: (i) the limited transmission of the reaction products through the FRS was accounted for by means of MOCADI simulations [16] and (ii) the detection efficiency at the final focal plane was determined. The contribution of those reactions that did not take place in the Be target, but in the materials surrounding it, should also be accounted for. Such a task required dedicated sets of measurements with an empty target, which could only be performed for a reduced number of cases. They showed a reduction of $30 \pm 10\%$ in the cross-section values. However, the lack of experimental data for Ne isotopes prevented a more accurate calculation.

In the high-energy regime, the one-neutron knockout channel is dominated by stripping reactions [13], where the last neutron is absorbed in the target and the $A-1$ core fragment is the sole

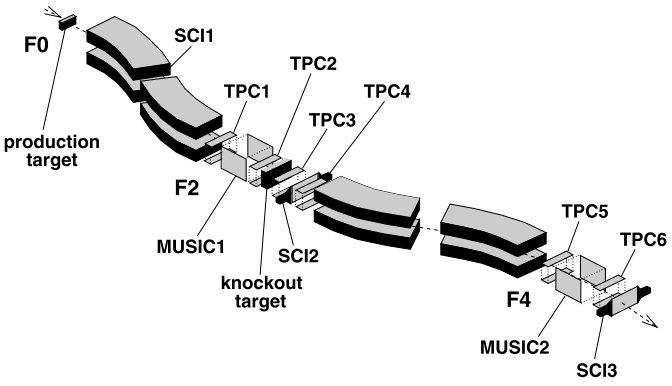

Fig. 1. Detector arrangement in the FRS magnetic spectrometer. The first stage of the FRS, F0–F2, was dedicated to select and identify the projectiles of interest. The reaction target (Be, 1720 mg/cm^2) was located at the intermediate focal plane, F2, and the one-neutron knockout fragments were studied in the second half of the spectrometer, F2–F4.

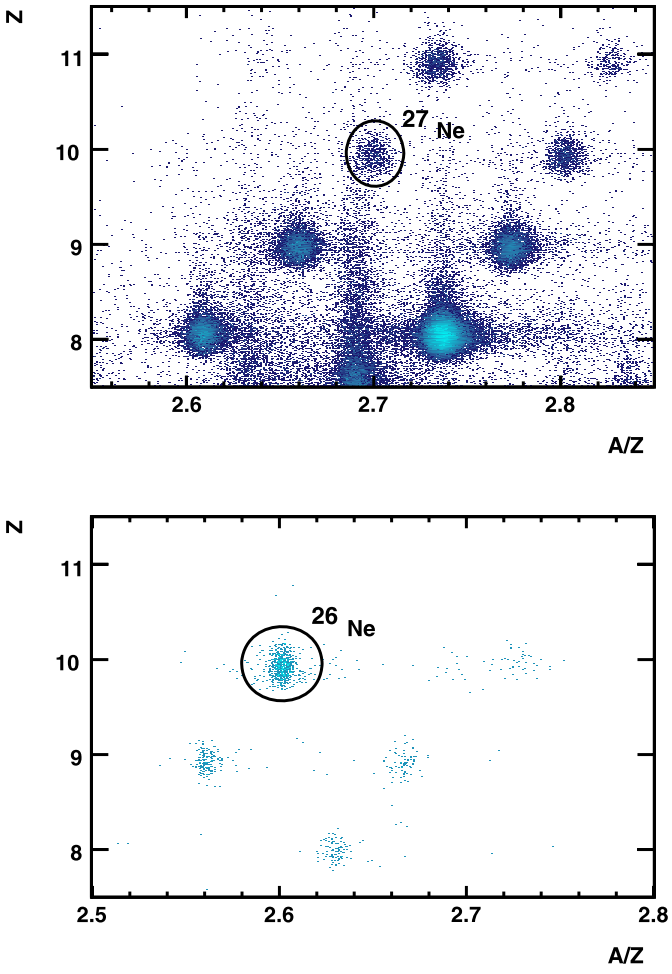

Fig. 2. (Top) Identification of incoming ^{27}Ne projectiles at the intermediate FRS focal plane. (Bottom) Outgoing ^{26}Ne fragments, after one-neutron knockout, at the final focal plane. It is demonstrated how the selection of ^{27}Ne projectiles at F2 automatically cleans the identification plot at F4, resulting in almost pure ^{26}Ne data. In general, for a given ^{A}X nucleus at F2, the corresponding $^{A-1}$X fragment at F4 was selected.

particle in the final state. Within this context, the momentum distribution of the fragment is usually identified with the ground-state distribution of the removed nucleon inside the projectile. This interpretation assumes that the target is *transparent* to the core

fragment and is commonly called *the transparent limit of the Serber model* [17]. However, the core survival implies that only the outer part of the wave function is sampled with this technique [18,19] and the observed momentum distributions are mainly determined by the asymptotic form of the wave function ($r \to \infty$), which, for a neutron with angular momentum l, can be written as follows:

$$\psi_{lm}(\mathbf{r}) \propto \kappa^{3/2} h_l(i\kappa r) Y_{lm}(\theta, \phi). \tag{1}$$

Here, θ and ϕ are the polar and azimutal angles, r is the module of the vector that connects the centre of mass of the core with the valence nucleon and $h_l(i\kappa r)$ represents the first spherical Hankel function. The parameter κ can be expressed in terms of the neutron-separation energy, S_n, and the reduced mass of the core-neutron system, μ, as $\kappa = \sqrt{2\mu S_n}$.

Momentum components transversal to the beam direction are much more affected by the reaction mechanism than the longitudinal one, which is regarded as a better way of exploring the projectile structure [20,21]. In order to obtain the probability distribution in the momentum space along the longitudinal z axis, the square Fourier transform of the wave function must be integrated over the transverse coordinates. One then obtains analytical expressions for the lowest angular momenta. A detailed description of this calculation can be found in Refs. [18,19]. The relevant components for the isotopes studied in this work are $l = 0$ and $l = 2$ and the associated longitudinal-momentum distributions, in terms of $k_z = \frac{p_z}{\hbar}$, are given by:

$$\frac{dN_{l=0}}{dk_z} = \frac{x_0^2 \kappa}{2\pi} \left\{ K_1^2(\xi) - K_0^2(\xi) \right\}, \tag{2}$$

$$\begin{aligned} \frac{dN_{l=2}}{dk_z} = \frac{x_0^2}{8\pi\kappa^3} \Bigg\{ & \left(3k_z^2 + \kappa^2\right)^2 \left[K_1^2(\xi) - K_0^2(\xi) \right] \\ & + 12k_z^2 \left(k_z^2 + \kappa^2\right) \left[K_2^2(\xi) - \frac{2}{\xi} K_1(\xi) K_2(\xi) - K_1^2(\xi) \right] \\ & + 3\left(k_z^2 + \kappa^2\right) \left[K_3^2(\xi) - \frac{4}{\xi} K_2(\xi) K_3(\xi) - K_2^2(\xi) \right] \Bigg\}, \end{aligned} \tag{3}$$

where K_{0-3} represent modified Bessel functions and their argument ξ is defined by Eq. (4)

$$\xi = x_0 \sqrt{k_z^2 + \kappa^2}. \tag{4}$$

The requirement of fragment survival is accounted for by means of x_0, interpreted as a lower cut-off on the impact parameter.

Eqs. (2)–(3) depend simply on the neutron-separation energy and on the selected cut-off parameter. They provide a useful tool for identifying the orbital angular momentum of the removed neutron because s and d waves can easily be distinguished from each other due to the significant difference in their characteristic widths.

4. Results

Table 1 summarises the one-neutron knockout cross-sections and the widths of the longitudinal-momentum distributions measured in the present experiment. According to the shell model, the last neutron of $^{24-28}$Ne isotopes would be described as $0d_{5/2}$ (^{24}Ne), $1s_{1/2}$ ($^{25-26}$Ne) and $0d_{3/2}$ ($^{27-28}$Ne). However, the Ne isotopes studied here are far from stability, with half lives ranging from 3.38 m to 20.0 ms, and predictions of the shell model need to be tested. This can be investigated by an appropriate analysis of the measured momentum distributions, since their widths contain information that provides us with a rough identification of $l = 0$ and $l = 2$ components participating in the configuration of those nuclei. The reduction of the width observed at $N = 15$ corresponds to the change from $0d_{5/2}$ to $1s_{1/2}$ configurations. This effect is accompanied by an enhancement of the cross-section, which can be understood within a simple picture where the neutron levels would be completely occupied up to $0d_{5/2}$ and a single neutron would stay in a $1s_{1/2}$ orbit. The filling of the $0d_{3/2}$ level is expected at $N = 17$ and should enhance the widths of the momentum distributions measured for $^{27-28}$Ne projectiles. However, the results obtained in this work seem to contradict this hypothesis.

Table 1
Inclusive one-neutron knockout cross-sections, σ_{-n}, and widths of the fragment longitudinal-momentum distributions as a function of the neutron number in the projectile, N. Cross-section values are not corrected for reactions that occurred outside the target, which give a contribution of about $30 \pm 10\%$.

Projectile	N	σ_{-n} (mb)	FWHM (MeV/c)
^{24}Ne	14	70 ± 8	207 ± 16
^{25}Ne	15	93 ± 10	149 ± 8
^{26}Ne	16	106 ± 11	135 ± 8
^{27}Ne	17	102 ± 12	122 ± 16
^{28}Ne	18	69 ± 8	105 ± 16

In order to develop a more accurate description of the $^{24-28}$Ne ground states, the experimental momentum distributions were carefully analysed using Eqs. (2)–(3). A simplified structure of the neon isotopes was assumed, uniquely based on two different $core(I^\pi, E) \otimes neutron(l)$ configurations, where I^π and E refer to the spin-parity and to the excitation energy of the core and l is the orbital angular momentum of the coupled neutron. On this basis, an admixture of two dN_l/dk_z components, each representing a $core \otimes neutron$ configuration, was used to fit the experimental momentum distributions and determine the ground state configuration of the projectiles. Calculations were done for several values of the cut-off parameter, x_0, looking for the minimum χ^2 and the best description of the experimental data. Fig. 3 gives an example of the quality of the fits.

The previous procedure provides the relative admixture of the selected dN_l/dk_z components. Results are summarised in Table 2 for the present analysis. The general trend of $^{24-26}$Ne isotopes is now expressed in a quantitative manner and clearly reflects the change from $l = 2$ to $l = 0$ configurations that takes place at $N = 15$. In the case of ^{27,28}Ne, with $N = 17$ and 18, an enhancement of the $l = 2$ component was expected due to the population of the $0d_{3/2}$ neutron orbital. However, as illustrated in Fig. 4 and Table 2, the analysis of the momentum distributions contradicts this hypothesis, showing that the ground state of these nuclei is dominated by $s_{1/2}$ neutrons coupled to an excited core. In particular, excited states of the core contribute with probabilities of 64 ± 12 and $81 \pm 9\%$ to the ground state of ^{27}Ne and ^{28}Ne, respectively.

It is interesting to compare the results for ^{26,28}Ne with the earlier one-neutron knockout experiment carried out by Terry et al. at NSCL [9], who based their conclusions on spectroscopic measurements performed with a segmented Ge array for γ detection. They obtained an accurate description of the projectiles, which accounted for the role of different excited states of the core. In particular, the $3/2^-$ intruder state of ^{27}Ne, at 765 keV, was populated in the one-neutron knockout of ^{28}Ne projectiles and constitutes a direct evidence of a intruder configuration in the ground state of ^{28}Ne.

In the work presented here, ^{26,28}Ne projectiles were described as the contribution of the ground state and the most probable excited level of the core [9]. This is a simplified picture that can be used to determine the role of excited core states in the projectile but does not distinguish between them. The comparison with the results given by Terry et al. should then be restricted to the

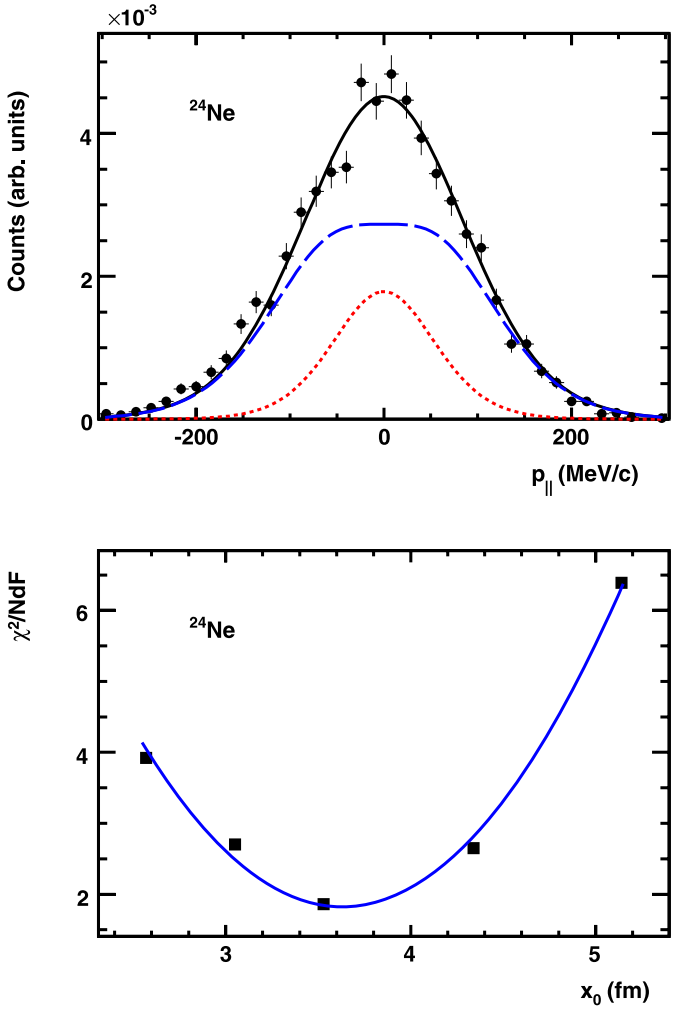

Fig. 3. (Top) Inclusive momentum distribution of ^{23}Ne after one-neutron knockout of ^{24}Ne (normalised to unity). The solid line represents the fit to the experimental data and the dotted (dashed) lines correspond to the calculated $l = 0$ ($l = 2$) contributions. (Bottom) Correlation between χ^2/NdF and the cut-off parameter, x_0, used to fit the experimental momentum distributions.

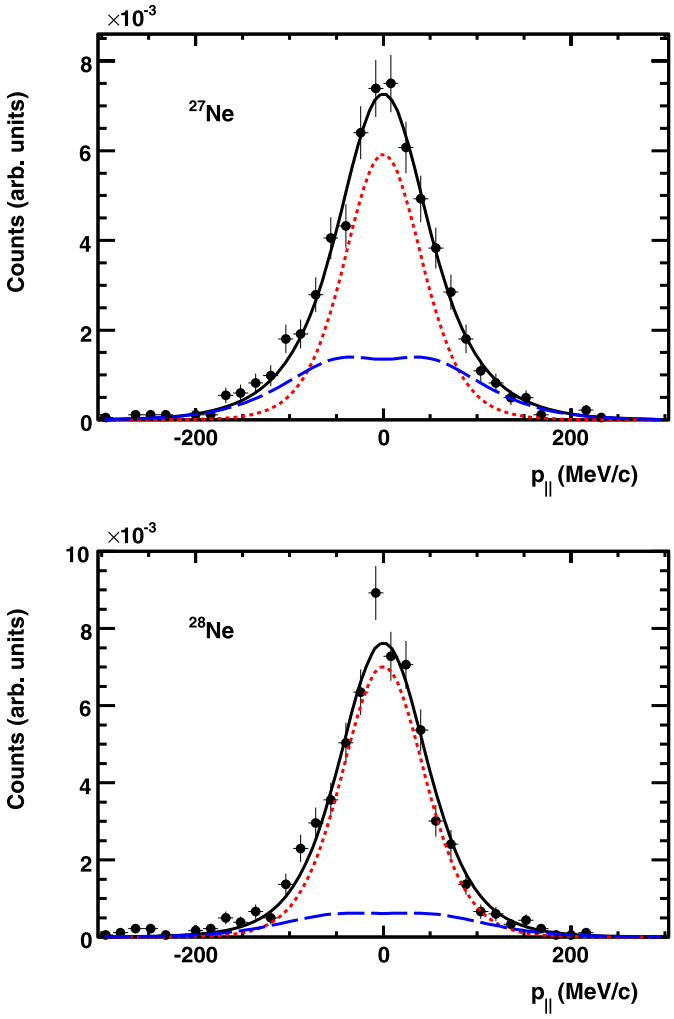

Fig. 4. Inclusive momentum distributions of ^{26,27}Ne after one-neutron knockout of ^{27,28}Ne (normalised to unity). The solid lines represent the fit to the experimental data. The dotted (dashed) lines correspond to the calculated $l = 0$ ($l = 2$) contributions.

Table 2
Calculated *core* ⊗ *neutron* contributions in the ground state of $^{24-28}$Ne. The lower cut-off for the impact parameter, x_0, is also included. E_{core} and I^{π}_{core} are the excitation energy and the spin-parity of the core fragment, l represents the orbital angular momentum of the coupled neutron and S_n corresponds to the standard one-neutron separation energy in the projectile [22] plus the excitation energy of the core.

Projectile	x_0 (fm)	E_{core} (keV)	S_n (keV)	I^{π}_{core}	l	Weight
^{24}Ne (0^+)	3.63 ± 0.12	0	8869	$5/2^+$	2	0.74 ± 0.05
		1017	9886	$1/2^+$	0	0.25 ± 0.05
^{25}Ne ($1/2^+$)	3.24 ± 0.11	0	4230	0^+	0	0.46 ± 0.03
		1982	6212	2^+	2	0.51 ± 0.03
^{26}Ne (0^+)	3.55 ± 0.13	0	5530	$1/2^+$	0	0.59 ± 0.03
		1703	7233	$5/2^+$	2	0.38 ± 0.03
^{27}Ne ($3/2^+$)	3.30 ± 0.47	0	1430	0^+	2	0.34 ± 0.11
		2024	3454	2^+	0	0.64 ± 0.12
^{28}Ne (0^+)	3.61 ± 0.50	0	3900	$3/2^+$	2	0.16 ± 0.08
		885	4785	$1/2^+$	0	0.81 ± 0.09

population of the core ground state in ^{26}Ne and ^{28}Ne one-neutron knockout, which, according to the present data, occurs with probabilities of 59 ± 3 and 16 ± 8%, respectively. Despite of using a different approach, there is an agreement between our results for the population of the core ground state and the 43% (^{26}Ne) and 32% (^{28}Ne) that are reported in Ref. [9].

5. Conclusions

The results presented here clearly show an enhancement of the $1s_{1/2}$ admixture in the ground state of ^{25,26}Ne, with $N = 15$ and 16. However, ^{27,28}Ne do not behave as expected. The valence neutron occupies a $1s_{1/2}$ level rather than $0d_{3/2}$ and is coupled to an excited state of the core. In order to study the structure of $^{24-28}$Ne projectiles in more detail, the measured momentum distributions were analysed on the basis of a simple theoretical model. Calculations included the orbital angular momentum of the removed neutron, its separation energy and a lower cut-off that acts on the impact parameter and ensures the core survival. A simplified picture of the projectile that accounted for only two possible *core* ⊗ *neutron* configurations was assumed and allowed to quantify the relative importance of core configurations in the ground and excited states. Conclusions derived from this description are

in good agreement with the exclusive results obtained by Terry et al. for ^{26,28}Ne one-neutron knockout. By and large, this work contributes to a better understanding of the neutron-rich region in the nuclear landscape and constitutes a valuable source of information in a domain that is still relatively unexplored.

Acknowledgements

This work was supported by: GSI, via Hochschulzusammenarbeitsvereinbarungen under contracts DA RICK, OF ELZ, MZ KRAK; FRBR under contract 08-02-012244; EC under contract ERBCHGE-CT92-0003; the Swedish Research Council and the Knut and Alice Wallenberg Foundation; Ministerio de Ciencia e Innovación under projects FPA2007-62681, FPA2007-62170; Ministerio de Educación under grant FPU-AP2005-3308 and the Galician Consellería de Educación e Ordenación Universitaria, Grupos de Referencia Competitiva 2006/46.

References

[1] C. Détraz, et al., Phys. Rev. C 19 (1979) 164.
[2] T. Motobayashi, et al., Phys. Lett. B 346 (1995) 9.
[3] Y. Utsuno, et al., Phys. Rev. C 60 (1999) 054315.
[4] T. Otsuka, et al., Nucl. Phys. A 682 (2001) 155c.
[5] T. Otsuka, Nucl. Phys. A 693 (2001) 383.
[6] R. Kanungo, Phys. Rev. Lett. 102 (2009) 152501.
[7] C.R. Hoffman, et al., Phys. Lett. B 672 (2009) 17.
[8] A. Obertelli, et al., Phys. Rev. C 74 (2006) 064305.
[9] J.R. Terry, et al., Phys. Lett. B 640 (2006) 86.
[10] B. Fernández-Domínguez, et al., Prog. Part. Nucl. Phys. 59 (2007) 389.
[11] M. Belleguic, et al., Phys. Rev. C 72 (2005) 054316.
[12] Z. Dombrádi, et al., Phys. Rev. Lett. 96 (2006) 182501.
[13] K. Hencken, G. Bertsch, H. Esbensen, Phys. Rev. C 54 (1996) 3043.
[14] H. Geissel, et al., Nucl. Instr. Meth. B 70 (1992) 286.
[15] http://www.gsi.de.
[16] N. Iwasa, et al., Nucl. Instr. Meth. B 126 (1997) 284.
[17] R. Serber, Phys. Rev. 72 (1947) 1008.
[18] P.G. Hansen, Phys. Rev. Lett. 77 (1996) 1016.
[19] M. Smedberg, Ph.D. thesis, Chalmers tekniska höskola och Göteborgs universitet, 1998.
[20] P.G. Hansen, A.S. Jensen, B. Jonson, Annu. Rev. Nucl. Part. Sci. 45 (1995) 591.
[21] C.A. Bertulani, K.W. McVoy, Phys. Rev. C 46 (1992) 2638.
[22] G. Audi, A.H. Wapstra, C. Thibault, Nucl. Phys. A 729 (2003) 337.